

PAPER • OPEN ACCESS

## Thermal and plasma enhanced atomic layer deposition of ultrathin TiO<sub>2</sub> on silicon from amide and alkoxide precursors: growth chemistry and photoelectrochemical performance

To cite this article: S O'Donnell *et al* 2022 *J. Phys. D: Appl. Phys.* **55** 085105

View the [article online](#) for updates and enhancements.

You may also like

- [Electrochemical Photocurrent X-Ray Spectroscopy: A Novel Analytical Surface Technique](#)  
Matthew James Strom, Donald F. Roeper, Paul M. Natishan *et al.*
- [Photocurrent Measurements of AlGaIn/GaN Hemit Under X-Ray Irradiation](#)  
Atsuki Miyata, Takuya Hoshii, Hitoshi Wakabayashi *et al.*
- [Developing Wrinkled Surface to Achieve Low-Cost Photoelectrochemical Biosensor and Study the Interplay between LSPR of Nanoparticles and Semiconductive Quantum Dots](#)  
Sudip Kumar Saha and Leyla Soleymani



The Electrochemical Society  
Advancing solid state & electrochemical science & technology

243rd ECS Meeting with SOFC-XVIII

**More than 50 symposia are available!**

Present your research and accelerate science

Boston, MA • May 28 – June 2, 2023

[Learn more and submit!](#)

# Thermal and plasma enhanced atomic layer deposition of ultrathin TiO<sub>2</sub> on silicon from amide and alkoxide precursors: growth chemistry and photoelectrochemical performance

S O'Donnell<sup>\*</sup> , F Jose, K Shiel, M Snelgrove , C McFeely, E McGill and R O'Connor 

School of Physical Sciences, Dublin City University, Dublin 9, Ireland

E-mail: [shane.odonnell42@mail.dcu.ie](mailto:shane.odonnell42@mail.dcu.ie)

Received 10 August 2021, revised 10 October 2021

Accepted for publication 3 November 2021

Published 16 November 2021



CrossMark

## Abstract

Due to its low cost and suitable band gap, silicon has been studied as a photoanode material for some time. However, as a result of poor stability during the oxygen evolution reaction (OER), Si still remains unsuitable for any extended use. Ultra-thin titanium dioxide (TiO<sub>2</sub>) films have been used as protective coatings and are shown to enhance Si photoanode lifetime with added solar to hydrogen performance improvements through distancing the oxidation reaction away from the Si photoanode surface and improved charge transport through the anode. This study details the nucleation, growth chemistry, and performance of TiO<sub>2</sub> thin films prepared via thermal and plasma enhanced atomic layer deposition (ALD) using both titanium isopropoxide and tetrakis(dimethylamido)titanium as the precursor material. The effect of post ALD treatments of plasma and air annealing was also studied. Films were investigated using photoelectrochemical cell testing to evaluate photoelectrochemical performance, and in-vacuum cycle-by-cycle x-ray photoelectron spectroscopy was used as the primary characterisation technique to study nucleation mechanisms and film properties contributing to improvements in cell performance. TiO<sub>2</sub> grown by plasma enhanced ALD results in cleaner films with reduced carbon incorporation. However, despite increased carbon incorporation, thermally grown films showed improved photocurrent as a result of oxygen vacancies in these films. Post deposition annealing in a H<sub>2</sub> ambient is shown to further improve photocurrent in all cases, while annealing in atmosphere leads to uniform film chemistry and enhanced photocurrent stability in all cases.

Supplementary material for this article is available [online](#)

Keywords: ALD, XPS, PEC water splitting, hydrogen, renewable energy

(Some figures may appear in colour only in the online journal)

\* Author to whom any correspondence should be addressed.



Original content from this work may be used under the terms of the [Creative Commons Attribution 4.0 licence](#). Any further distribution of this work must maintain attribution to the author(s) and the title of the work, journal citation and DOI.

## 1. Introduction

With the acceleration of climate change events comes an increasing urgency and demand for more sustainable forms of energy production going forward. In order to move away from the long-established sources of energy from fossil fuels, a new green energy mix must be developed. One alternative which has been highlighted as a promising solution is the production of hydrogen fuel through the capture and conversion of solar energy. This involves the conversion of incoming photons to a form of chemical energy through the dissociation of water molecules into their constituent parts, hydrogen and oxygen. As such, over the last 50 years, the use of semiconducting materials as both light-absorbers and energy converters as a route to direct solar water splitting has been an active area of research.

The process of water splitting for hydrogen production is often referred to as artificial photosynthesis, wherein incoming solar energy is converted to chemical energy through the dissociation of water into hydrogen and oxygen [1]. The basis for the operation of photoelectrochemical systems is the semiconductor photoelectrode, and the material chosen to fill this role. To offer any viability the material must fulfil several requirements simultaneously, namely: effective charge separation and transport,  $H_2$  or  $O_2$  evolution at its surface, along with suitable light absorption [2]. In addition, it must be highly stable in aqueous solution and cost effective in order to make photoelectrochemical water splitting a viable competitor to the established fossil fuels used presently. No single semiconducting material has been identified to satisfy all of these requirements as yet, leading to the development of composite photoelectrode materials which serve individual roles to achieve the same goal [2].

Si, GaAs and GaP possess characteristics which make them possible candidates as potential photoanode materials for the development of water splitting architectures owing to their suitable light absorption properties and band edge positions which facilitate the water oxidation half—reaction [1]. However, these materials suffer badly from oxidation in electrolyte solutions during the oxygen evolution reaction (OER) due to the oxidation of the electrode material itself competing with the oxidation of water resulting in their passivation thus rendering them dysfunctional in too short of a timespan to be of any use in large scale energy conversion [3–5]. The oxidation reaction causes photo corrosion of the anode material impeding the desired water oxidation process thus causing the electrode surface to become either passivated or corroded upon illumination.

Thus, it has become clear that the anode material must be coated with a protective layer which will limit or eliminate the degradation effects in order to extend the lifetime of the materials and potentially enhance photocurrent output by acting as catalyst for the OER. In recent years, titanium dioxide ( $TiO_2$ ), initially itself studied as a photo-anode [6] has emerged as a promising candidate for protecting silicon photoanodes, leading to a considerable amount of research interest into its viability [4, 7–9].  $TiO_2$ , when applied in layers sufficiently thin such as not to obstruct light absorption, is of particular interest as

a protective material for silicon photoanodes as a result of its optical transparency owing to its large band gap, along with good stability over a range of pH values [10].

The requirements of a protective layer are that it is sufficiently thin to allow most of the incident light to reach the photoanode surface and allow for effective hole transport to the electrolyte interface, while also being highly resistant to corrosion. Atomic layer deposition (ALD) is ideally suited for the deposition of protective layers such as  $TiO_2$  due to the conformal and high-quality nature of films grown via this technique [11]. ALD is a vapor-phase deposition technique which uses discrete alternating self-limiting reactions of gas phase reactant and co-reactant species which allow for the growth of films of a desired thickness one atomic layer at a time. This method of film growth allows for the formation of thin and ultra-thin films with precise control over composition through the tunability of the ALD process [12].

One of the key goals of this work is to determine the extent to which the ALD process and precursor chemistry impacts on the resulting  $TiO_2$  film and its photoelectrochemical performance. A number of  $TiO_2$  ALD precursors have been reported upon in the literature, with titanium tetrachloride ( $TiCl_4$ ) being perhaps the most common [10, 13, 14]. However, corrosive by-products from the process limit its potential for large scale uptake. Bronneberg *et al* have reported on a cycle-by-cycle study of the nucleation and growth of thin films of  $TiO_2$  on silicon using thermal ALD with  $TiCl_4$  and  $H_2O$  as the co-reactant. In this work we present an in-line x-ray photoelectron spectroscopy (XPS) analysis of the nucleation and growth of ultra-thin (ca. 2 nm)  $TiO_2$  films on silicon from two ALD precursor molecules, titanium isopropoxide (TTIP) and tetrakis(dimethylamido)titanium (TDMAT). Our work particularly focuses on the impact of precursor choice, and the use of thermal ALD (T-ALD) vs plasma-enhanced ALD (PE-ALD), on the chemistry of the produced films, and how this impacts the photoelectrochemical performance of silicon photoanodes.

In this study, ALD of  $TiO_2$  was performed in a unique, custom-designed Oxford Instrument ALD reactor which is coupled in-vacuum to a Scienta Omicron monochromated XPS by a fast-transfer robotic handler. This setup allows for rapid cycle-by-cycle XPS analysis of the ALD films during nucleation and growth, and a robust comparison of process parameters.

Our results show significant differences in film chemistry between PE-ALD and T-ALD recipes, including reduced ligand incorporation and increased interaction with the underlying silicon identified as titanium suboxide formation during PE-ALD. There are also subtle differences between the chemistry of the films resulting from the two precursors.

Photoelectrochemical testing also shows some differences in photo-current between the processes. In all cases, following an appraisal of the photo-electrochemical performance of the as-deposited layers, the films were exposed to a post deposition  $H_2$  plasma anneal and a high-temperature air anneal in order to examine the effect of annealing on the individual ALD films, and how the annealing impacts photoelectrochemical performance and stability. Results show good correlation to

**Table 1.** ALD deposition parameters detailing individual process recipes.

Variable	TDMAT plasma	TDMAT thermal	TTIP plasma	TTIP thermal
Precursor Dose (s)	0.5	1	2	2
Precursor Purge (s)	3	5	6	5
Co-reactant Dose (s)	4	0.15	5	0.15
Co-reactant Purge (s)	2	10	4	20
Substrate Deposition Temperature (°C)	270	250	270	250

those observed by Hannula *et al* for much thicker (ca 30 nm) films.

## 2. Experimental

### 2.1. ALD of TiO<sub>2</sub>

TiO<sub>2</sub> films were deposited on n-Si(100) ( $\rho = 5 - 9 \Omega \text{ cm}^2$ ). Samples were cut from the wafer in  $2.5 \times 2.5 \text{ cm}^2$  coupons. Prior to ALD processing, samples were exposed for 5 min to a 300 W remote H<sub>2</sub> plasma in the deposition chamber to remove adventitious carbon and increase surface hydroxyl groups to improve nucleation during the ALD process. XPS elemental compositions carried out on samples before H<sub>2</sub> plasma treatment exhibited approximately 8% C 1s contribution owing to atmospheric contamination of the Si substrates. Following H<sub>2</sub> plasma treatment this C 1s contribution is beyond the detectable limits of the XPS.

ALD took place in an Oxford Instruments FlexAl ALD Reactor (base pressure  $3.8 \times 10^{-7}$  Torr), using TTIP (Sigma Aldrich 97%) and tetrakis(dimethylaminol) titanium (TDMAT, Sigma Aldrich 99.999%) as precursors and H<sub>2</sub>O and O<sub>2</sub> Plasma as co-reactants for T-ALD and PE-ALD, respectively. A longer dose time for TTIP was implemented to ensure sufficient precursor entered the growth chamber. Literature reports state the vapour pressure for TTIP to be between 0.59 and 8.4 Torr for precursor delivery temperatures of 60 °C–100 °C with this falling to as low as 0.02 Torr for lower temperatures of 25 °C [15]. With TDMAT being reported to have a vapour pressure of 0.5 Torr at approximately 50 °C [16]. The substrate was heated to 270 °C and 250 °C for plasma and thermally grown films, respectively. The plasma source used for purposes of deposition and post-treatment annealing is an RF generated ICP source with an excitation energy of 13.56 MHz. Post-deposition plasma annealing was performed using H<sub>2</sub> plasma at 300 W for 5 min. Air annealing of films was carried out at 500 °C for 1 h using a Nabertherm furnace in ambient air. The recipes, as shown in table 1, were designed based on the ALD tool manufacturer's optimized recipes. Bubbler and purge flows were carried out using continuously flowed Ar at 100 sccm and 200 sccm respectively. Resulting growth rates are reported in the section 3.

### 2.2. Characterisation techniques

The primary characterisation technique employed in this work is XPS, which allowed for chemical composition and thickness

determination of the TiO<sub>2</sub> films. XPS was performed using a Scienta Omicron XPS (Monochromated Al K $\alpha$  source, base pressure of  $6.5 \times 10^{-7}$  Pa) with a 128 channel Argus CU detector. The XPS is coupled in-vacuum by a robotic wafer handler allowing for sample transfer from ALD to XPS in approximately 1 min without the need for breaking vacuum. Survey scan and high-resolution spectra were taken at normal emission from the sample using 1 and 0.1 eV step sizes, respectively. All spectral fits utilised a Shirley–Sherwood type background in conjunction with Voigt profiles. XPS data analysis was carried out using analyzer fitting software with photoemission peaks shifted in accordance with the Si<sup>0</sup> 2p<sub>3/2</sub> signal at 99.4 eV binding energy (BE) [17, 18].

Thickness values were extracted from the XPS spectra using the Thickogram method [19], which is a quick and accurate method of determining film thickness using the suppression of the substrate signal. Developed as a method to derive film thickness from data of the film and sample substrate peak intensities at a given take off angle, the Thickogram can be applied in a graphical or a mathematical approach. Effective attenuation lengths (EALs) were obtained from the NIST EAL database and XPS relative sensitivity factors were taken from the database of empirically derived atomic sensitivity factors, by Wagner *et al* [20, 21]. Film thicknesses using this method were cross referenced against values extracted by ellipsometry and were in-agreement with expected thicknesses based on anticipated growth per cycle (GPC) rates as indicated by ALD recipes from the tool manufacturer. Spectroscopic ellipsometry was carried out for thickness verification on the films using a Woollam XLS-100 multi-wavelength system.

The experiments in this work were designed to probe the early-stage growth and nucleation mechanisms through sequential growth of films which involves performing a half cycle of ALD followed by a suite of XPS scans up to a total of two full cycles. Following this, three full cycles are executed, followed by another suite of XPS scans. Finally, repeated batches of ten complete cycles are carried out followed by XPS scanning up to a final sum of 65 cycles. This methodology was chosen as it gave a good insight into the early-stage growth while avoiding overly granularizing the data by scanning after every half cycle and resulted in a film thickness of approximately 2 nm.

Photoelectrochemical performance was studied using TiO<sub>2</sub> layers grown via the four deposition processes in a continuous deposition. Several thicknesses were deposited and studied; however, the focus of this work is on 2 nm films, which emerged as the optimal thickness when electrochemically

tested, being suitably thin to allow light transmission and hole transport to the electrode surface, while simultaneously offering anode protection.

Photoelectrochemical cell testing was carried out in a Redoxme AB MM 15 ml double-sided photoelectrochemical cell with a Pt counter electrode (99.9%) and a Ag/AgCl (1 mol KCl) reference electrode. The electrolyte was a 0.5 M phosphate buffer solution (pH 7.4). The electrodes were irradiated with  $1000 \text{ W m}^{-2}$  AM 1.5 G simulated sunlight from an Oriol Instruments xenon arc lamp solar simulator in a top-down configuration with  $1 \text{ cm}^2$  of illuminated sample area during testing. Linear sweep voltammetry ( $I$ - $V$ ) testing is performed for the acquisition of key photoanode material characteristics such as photocurrent density, onset potential and dark current outputs as a function of an applied potential [2]. In this study, samples were studied under constant illumination and tested from 0 to 4.17 V vs reversible hydrogen electrode (RHE). In addition to this linear sweep voltammetry, chronoamperometric detection was also carried out on separate samples to those which had been  $I$ - $V$  tested. Amperometry involves the application of a constant potential to a working electrode and the measurement of the output steady-state current [22]. Samples in this work were subjected to a constant potential of 1 V vs Ag/AgCl corresponding to 1.67 V vs the RHE, for 100 s which offers some insight into the potential durability of the photoanodes.

Morphological images were obtained using a Bruker Icon atomic force microscope (AFM) in tapping mode operation. Data were collected from a surface area of  $1 \times 1 \mu\text{m}^2$  at 256 Samples/Line. Studies were performed in air using Si cantilevers with a 30 nm Al reflex coating with a tip radius of  $<10 \text{ nm}$ . Acquired AFM and root mean squared (RMS) surface roughness were treated by Gwyddion analysis software [23].

Grazing-angle ATR FTIR was performed using a Nicolet iS50 FTIR Spectrometer in conjunction with a Harrick VariGATR attachment. The germanium crystal was cleaned using butanone which removed any contaminants prior to a background scan being taken. Samples were placed face down on the crystal and a force of  $\sim 700 \text{ N}$  was applied to ensure good contact between the sample and crystal. A total of 128 scans were performed per sample at an  $8 \text{ cm}^{-1}$  resolution with an unpolarized angle of incidence of  $65^\circ$ . FTIR is an established technique for the study of molecular vibrations. Deposited films were investigated using this technique in order to determine the presence of and variations of molecular vibrations of  $\text{TiO}_2$  thin films such as hydroxyl groups [24].

### 3. Results and discussion

#### 3.1. FTIR

Figure 1 shows the FTIR absorbance spectra for the four-deposition processes *as-deposited*. The four deposition processes consist of growing 2 nm films using both TDMAT and TTIP via thermal and plasma enhanced ALD. Resulting FTIR spectra are similar for all  $\text{TiO}_2$  growth processes. Marginal deviations are observed in carbon and oxygen bonding with additional C=O observed in TDMAT PE-ALD which

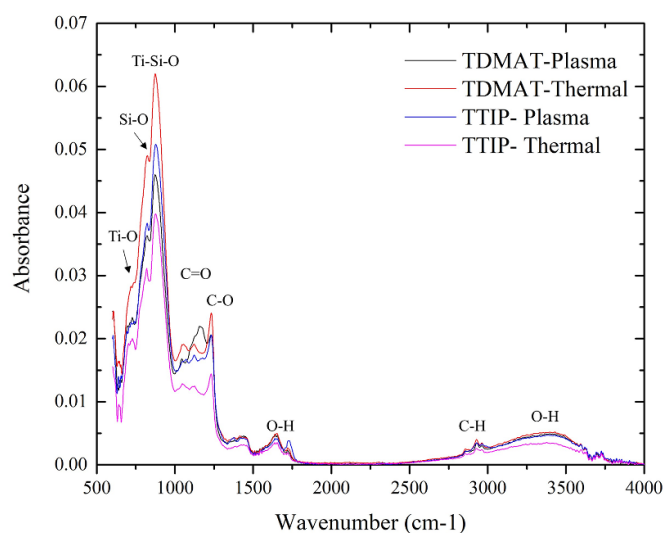


**Figure 1.** FTIR spectra of as-deposited  $\text{TiO}_2$  films from all deposition processes.

correlates with XPS analysis of the C1s region shown later in this study.

The dominant peak in the spectra shown in figure 1 occurs at  $877 \text{ cm}^{-1}$ , representing Ti-O-Si bonds, which confirms a chemical interaction between the deposited  $\text{TiO}_2$  films and the underlying  $\text{SiO}_2$  [12]. The shoulder feature at  $728 \text{ cm}^{-1}$  corresponds to Ti-O bonds with Si-O observed at  $825 \text{ cm}^{-1}$  [12]. A peak at  $1172 \text{ cm}^{-1}$  is attributed to C-O stretching bonds linked to the  $\text{TiO}_2$  film. The spectrum features peaks at  $1452 \text{ cm}^{-1}$  and  $1644 \text{ cm}^{-1}$ , which are in line with expected values for OH groups (hydroxyls) [12]. These peaks indicate the chemisorption of O-H molecules in the deposited  $\text{TiO}_2$  overlayer. The broad band from  $3000$  to  $3640 \text{ cm}^{-1}$  also indicates strong interactions through hydrogen bonding between the  $\text{TiO}_2$  film and surface hydroxyls [12].

#### 3.2. XPS

XPS analysis was carried out on samples as-loaded as well as following a plasma cleaning step prior to ALD to prepare samples for deposition. In addition to this, samples were later subjected to annealing treatments both *in* and *ex-situ* and again photoemission analysis was performed to study effects of the post-deposition treatments. As-deposited samples were analysed using AFM to check for agglomerations on the film surfaces and also showed highly uniform surfaces with RMS roughness of 103 pm, 144 pm, 88 pm and 178 pm for TDMAT plasma grown (TD-P), TDMAT thermally grown (TD-T), TTIP plasma grown (TT-P) and TTIP thermally grown (TT-T) respectively (see figure S1 available online at [stacks.iop.org/JPD/55/085105/mmedia](https://stacks.iop.org/JPD/55/085105/mmedia)). While mean roughness values were as follows; 74 pm, 109 pm, 70 pm and 142 pm for TD-T, TD-T, TT-P and TT-T respectively.

In order to achieve an understanding of the early-stage growth kinetics for each process and for accurate determination of GPC rates, sequentially grown films were deposited and subsequently analysed using the integrated XPS. Attention

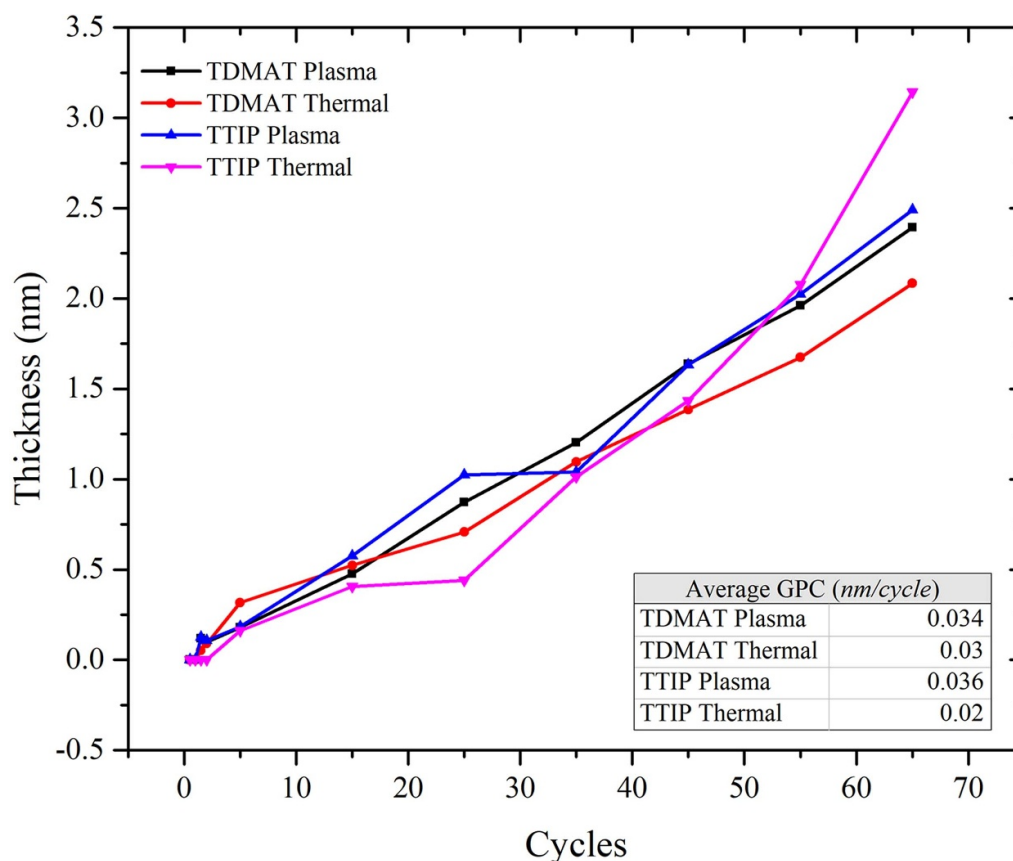


**Figure 2.** Sequentially grown ALD TiO<sub>2</sub> films for four processes investigating the evolution of the GPC for the various recipes as per table 1.

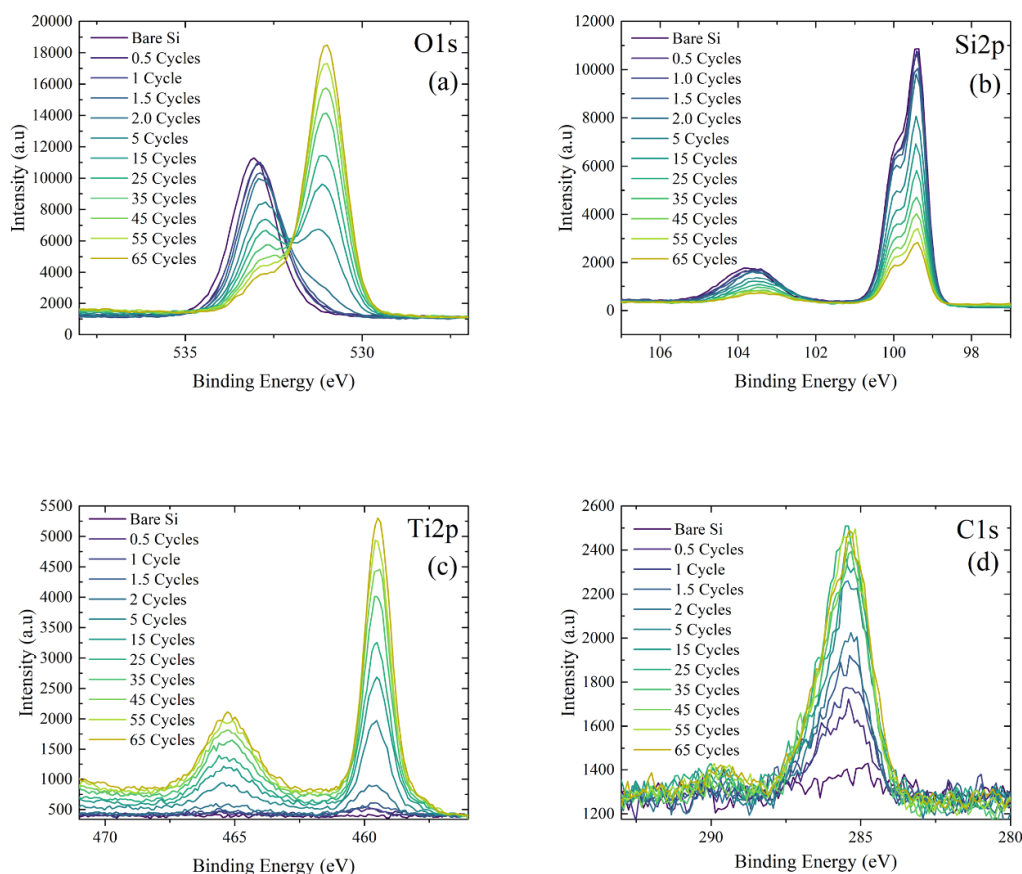
was focused primarily on the Si 2p, Ti 2p, C 1s and O 1s core levels to monitor for any development of additional oxidation states in the case of Ti 2p or evidence of titanium silicate formation for low cycle numbers in the Si 2p peak. This is particularly important, as hole transport to the electrode surface will rely heavily on the quality and chemistry of the interface between the TiO<sub>2</sub> film and the underlying silicon.

Figure 2 shows the GPC for all four processes as-deposited. More consistent, linear early-stage growth is observed for PE-ALD processes. Additionally, thermally grown TTIP displayed evidence of nucleation delay and subsequent enhanced growth in the latter stages. Thicknesses were determined using the Thickogram method, and verified with ellipsometry [19]. These sequential-growth depositions were used to investigate the early state growth characteristics and allowed for the determination of exact growth rates for each process. These GPC rates were used later for precise thickness deposition for purposes of photoelectrochemical cell testing wherein accurate film thickness is necessary to accurately compare the processes. In all cases, XPS growth rates were cross referenced with those obtained through spectroscopic ellipsometry.

Figure 3(a) shows the evolution of the O 1s peak as a function of increasing number of ALD cycles for the TDMAT thermal process. In this figure, two dominant oxygen peaks are observed, the first being oxygen in SiO<sub>2</sub> at a BE position

at approximately 533 eV and the second is oxygen in TiO<sub>2</sub> at approximately 531 eV. Figure 3(b) shows the Si 2p evolution, where the SiO<sub>2</sub> peak is seen to attenuate rapidly, due to suppression of the substrate signal during the growth of the TiO<sub>2</sub> overlayer. Also, in figure 3(b) we see a shifting of the silicon oxide peak towards lower BE as the number of cycles increases suggesting the formation of silicon suboxides or titanium silicate at the interface, as suggested in figure 1. Figure 3(c) shows the sequential growth of the Ti 2p region. Growth can be seen to initiate as early as after the first half cycle of the sequential deposition with consistent peak evolution observed throughout. In the case of the T-ALD processes for both TTIP and TDMAT, a low BE shoulder is seen to form as early as five cycles into the deposition, attributable to titanium in the 3+ oxidation state. Figure 3(d) shows the C 1s as a function of cycle number, with an increase in carbon composition with increasing cycles, despite the film not leaving vacuum between ALD and XPS analysis. Having started from a clean H<sub>2</sub> plasma treated samples surface with negligible carbon contribution, the C 1s region grows steadily leaving a significant composition after 65 cycles of approximately 16% for this particular process. Figures of the remaining TDMAT and both TTIP processes high resolution images are shown in figures S2–S4.

In order to further illustrate the complications in interpreting carbon and oxygen spectra that can be avoided by analysing ALD processes without breaking vacuum, figure 4 shows



**Figure 3.** Thermal TDMAT sample evolution as a function of increasing number of ALD cycles depicting the change in composition as the thickness of the titanium overlayer increases. (a) Evolution of the O 1s photoemission peak as it changes from a SiO<sub>2</sub> dominant peak to TiO<sub>2</sub> dominant. (b) Attenuation of the SiO<sub>2</sub> peak is shown. (c) Ti 2p region showing peak intensity increase with increasing cycles. (d) C 1s peak showing remnant carbon incorporation in the film.

an example of a 2 nm TiO<sub>2</sub> layer which was scanned post deposition and following exposure to atmosphere for 5 min. The as-deposited sample shows a significant carbon signal. Once exposed to atmosphere there is a further growth in the C 1s. Note however that the growth of adventitious carbon can mask the carbon associated with ligand incorporation, though many works attribute the entirety of the C 1s peak area to adventitious carbon. In many processes, up to 30% carbon can be observed which, if incorporated in the film will significantly impact the material properties and the suitability of the ALD process under investigation [25]. In this work, all growth processes show less than 20% carbon within the film as a result of remnant ligands trapped during the deposition. Depth profiling of ALD films with XPS is often carried out using Ar-ion sputtering, but given the ion beam's tendency to change the film's structure as it removes material, this is not a wholly reliable indicator of the chemical composition of bulk films [26, 27]. The degree of incorporation of the ligands in our films is evident in figure 3(d) with the sequential deposition of a TiO<sub>2</sub> film and the steady growth of the C 1s peak. The observation in figure 3(d) which suggests continuous carbon incorporation is expanded upon in figure 5 which details the carbon concentration as a function of the number of cycles observed in the sequentially grown films for all process. From

a theoretical viewpoint during an ideal ALD process, on every oxidant pulse remnant CH<sub>3</sub> groups of the TTIP and TDMAT molecules respectively should be removed. It is already clear from figure 5 that this is not the case given the consistent growth of the carbon peak throughout the deposition for all processes. Elemental compositions for all film growth processes and post-deposition annealing treatment are available in the supplemental information, see table T1. One point to note is that there appears to be reduced ligand incorporation in the PE-ALD grown layers when compared to T-ALD as is seen from their overall lower relative sample carbon content and the rate at which the carbon contribution in these plasma grown samples stabilizes.

Following the sequential depositions detailed above, a series of conventional depositions were performed to confirm GPC values and to confirm consistency of the TiO<sub>2</sub> deposition processes. A temperature of 270 °C was selected for sample temperature which is within the ALD window for both TDMAT and TTIP which provided suitable growth rates and minimal remnant carbon ligands from the ALD process [12]. From this point forward all XPS BE positions and electrochemical measurements discussed pertain specifically to the straight-through 2 nm thick layers as opposed to those grown sequentially.

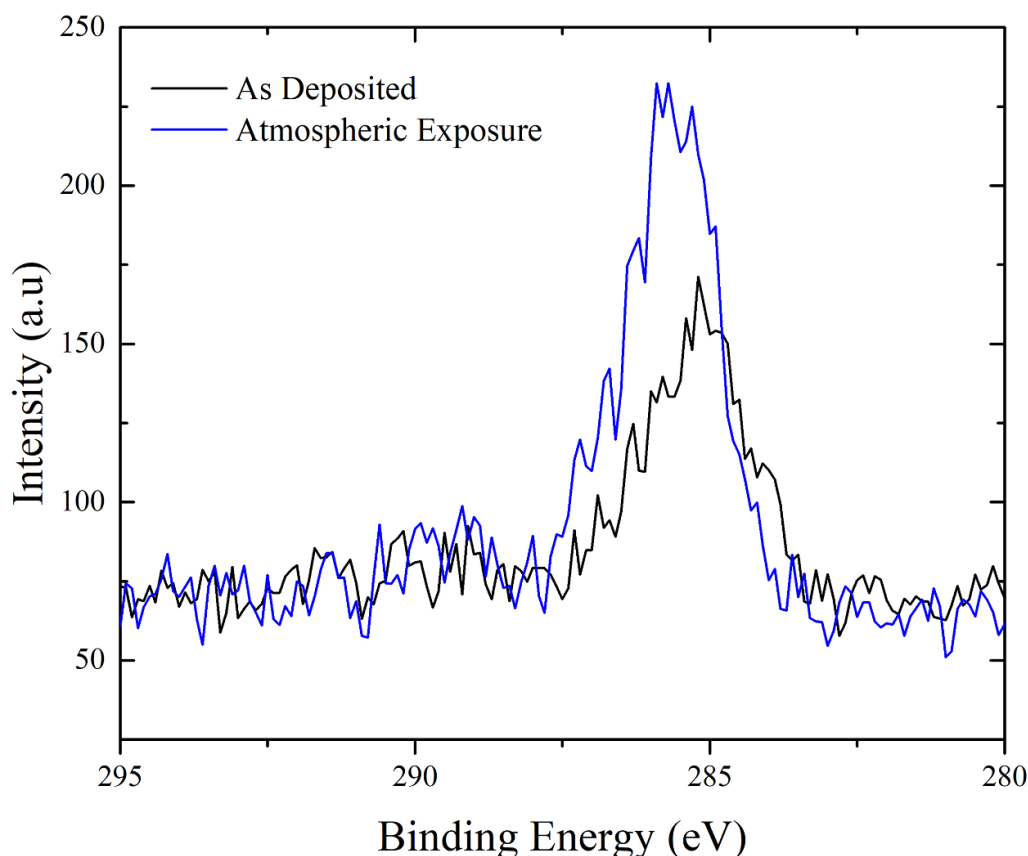


**Figure 4.** High resolution XPS spectra for the C 1s region showing the carbon contribution of a TiO<sub>2</sub> film grown using TDMAT PE-ALD at two stages: as-deposited and post atmospheric exposure, showing the importance of *in-situ* studies of ALD films.

As shown in figure 6, for both PE-ALD processes, Ti was present only in the Ti<sup>4+</sup> state with TDMAT plasma (TD-P) at 458.9 eV and TTIP plasma (TT-P) at 459.2 eV which are consistent with previous reports [1, 28–30]. This is in contrast to the T-ALD processes which show the presence of Ti<sup>3+</sup> at 458.2 eV and 458.1 eV for TDMAT (TD-T) and TTIP (TT-T) respectively in addition to Ti<sup>4+</sup>. The literature indicates the BE position of Ti<sup>3+</sup> to be in the region of 1.3–2.3 eV lower than Ti<sup>4+</sup> [28–30]. The measured spin orbit splitting for the TD-P, TT-P and TT-T is 5.7 eV with the TD-T found to be 5.18 eV, again consistent with values reported in the literature [28, 29]. High resolution Ti 2p spectra were fitted as two singlet peaks, with the peak area of the Ti 2p<sub>1/2</sub> being 0.43 of that of the Ti 2p<sub>3/2</sub> rather than the traditional 0.5 and the FWHM of the Ti 2p<sub>3/2</sub> being higher, a similar method being implemented by Hannula *et al* [1]. This approach is taken to account for the Coster–Kronig effect which leads to a difference in the peak width of two spin-orbit doublet peaks which occurs in 2p spectra of first row transition metals [1, 31]. In addition to this, the TT-T spectra required an additional oxide peak at 457.8 eV in order to improve the fit. This TT-T sample is the only one of the processes which is seen to contain this peak directly following depositions and its BE is in line with reports for the presence of Ti<sup>2+</sup> [29]. Figure 6(a) shows the fitted Ti 2p peaks for all four processes which shows the good quality single state nature of PE-ALD grown films in contrast

with the T-ALD films which exhibit 3+ and in some cases 2+ states.

Samples with Ti<sup>3+</sup> present exhibited a blue tint when compared to those without it, this result is due resulting from d–d transitions as described by Di Valentini *et al* [32, 33]. An exemplar fitted spectrum of a T-ALD grown sample using TDMAT as the precursor is shown in figure 6(b) which clearly shows the presence of the Ti<sup>3+</sup> state.

### 3.3. Post deposition treatment

Using the established growth rates, we deposited films of 2 nm for purposes of electrochemical testing and XPS characterisations. These thicknesses were grown in a straight through deposition wherein the ALD process continues uninterrupted to a desired number of cycles as per the required calculated number based on the previously calculated growth rates.

Once depositions had been complete for each process and the samples were scanned with XPS to verify thickness and composition, they were removed from vacuum and stored in atmosphere prior to receiving subsequent annealing treatments.

In order to understand the effects of annealing in oxidizing and reducing ambients on the thin TiO<sub>2</sub> films, high temperature anneals were carried out both in atmosphere, and in H<sub>2</sub> plasma under vacuum, respectively. Upon being reinserted



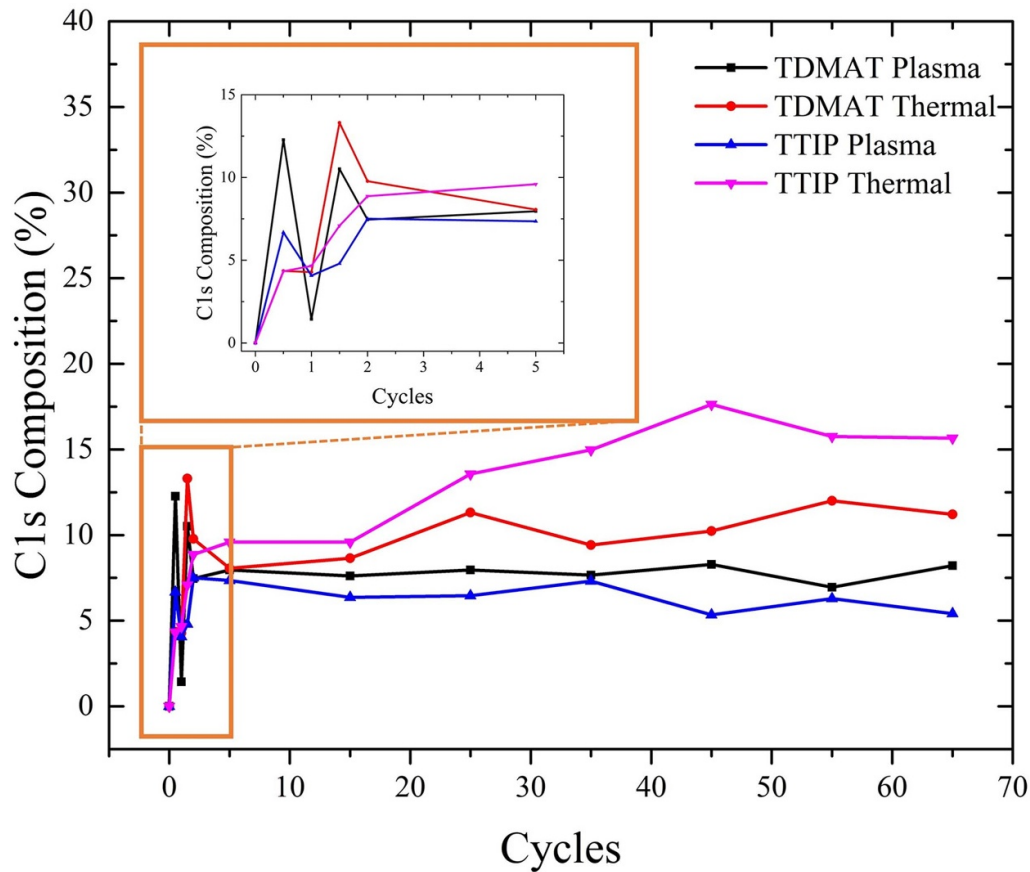


**Figure 5.** Carbon composition of TiO<sub>2</sub> films as a function of number of cycles sequentially grown with an enhanced view of the early-stage cycles up to five cycles total.

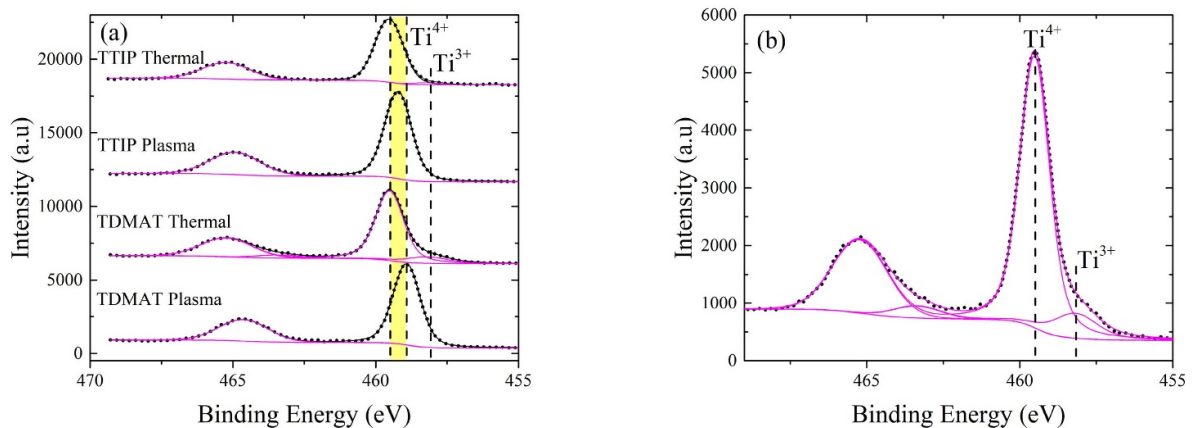


**Figure 6.** (a) Comparative figure of four processes showing Ti 2p fits and (b) Ti 2p high resolution photoemission peak from TDMAT thermally grown film showing the presence of Ti<sup>3+</sup>.

into the ALD-XPS system for H<sub>2</sub> plasma annealing, XPS scans were performed on all samples to determine their reaction to atmospheric exposure prior to annealing. Once annealed, samples underwent additional photoemission analysis to study the effect of the H<sub>2</sub> treatment. Given that the performance of the TiO<sub>2</sub> films in atmosphere is of interest, it is important to understand the surface chemistry of the TiO<sub>2</sub> when it has been re-exposed to atmosphere following the H<sub>2</sub> annealing step. As the samples are so thin, one may expect partial,

or full re-oxidizing of the reduced films upon atmospheric exposure. Therefore, samples were moved to the system load lock where they were exposed to atmosphere for 5 min before being loaded once more to vacuum for a final XPS scan.

Firstly, addressing the samples post—H<sub>2</sub> plasma anneal but prior to exposure to atmospheric conditions (figure 7), the Ti 2p peak showed the presence of the Ti<sup>2+</sup> state at 457 eV for all process along with the aforementioned Ti<sup>4+</sup> and Ti<sup>3+</sup> states at the previously mentioned binding energies which dominate

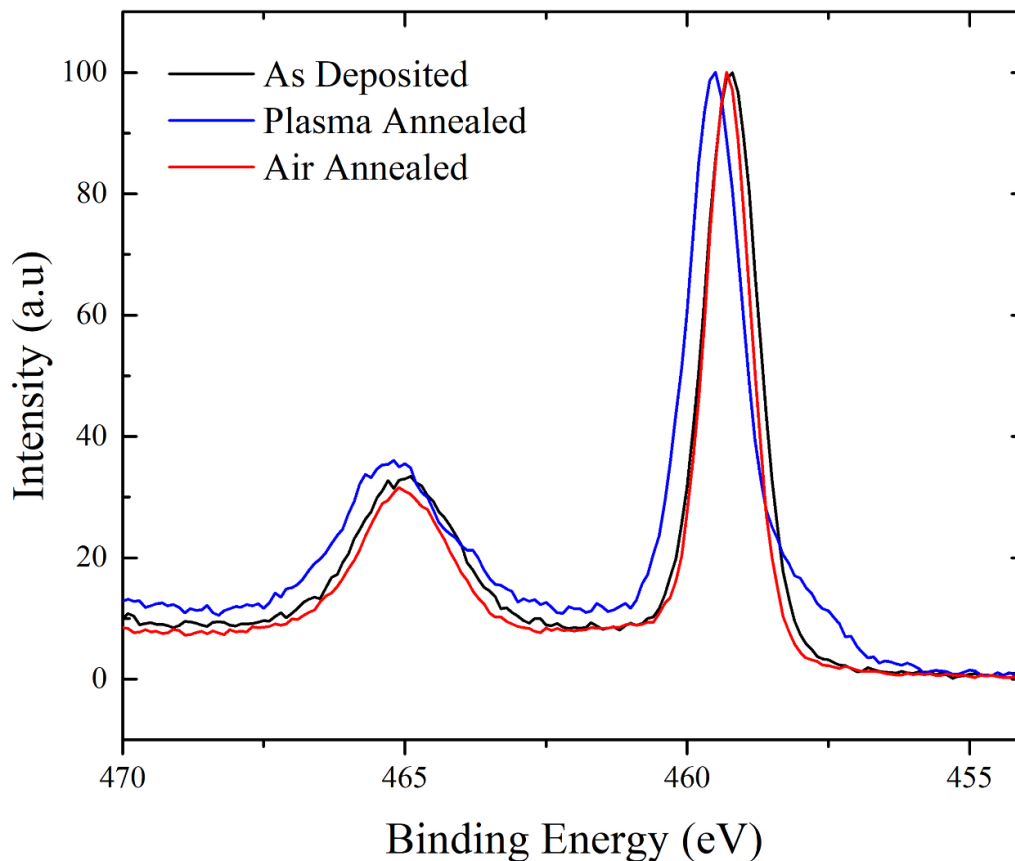


**Figure 7.** High resolution XPS scan of the Ti 2p region showing all stages of treatment for a TTIP plasma grown sample.

the spectra. In all cases  $Ti^{4+}$  is the dominant species followed by  $Ti^{3+}$  and then  $Ti^{2+}$ .

Following subsequent exposure to atmosphere all samples see a drastic decrease in  $Ti^{3+}$  and  $Ti^{2+}$  components with their composition being made up almost entirely of  $Ti^{4+}$ . This is key information from an *in-situ* perspective as it shows the true state of the titania films in atmosphere following plasma annealing and the significant degree of re-oxidation upon atmospheric exposure. An example of the effect of annealing treatments is shown in figure 7 where TTIP plasma grown titanium films at all stages of treatment show the change in state of the Ti 2p state for each stage. The remaining growth processes at all stages of treatment are shown in figure S8 and shows that PE-ALD grown plasma annealed samples remain at higher BE compared to the as-deposited and air annealed samples due to the main formation of silicates having taken place during film growth. Following  $H_2$  plasma annealing we see a partial conversion of the Ti–Si–O back to titanium in its  $4^+$  oxidation state, this effect is corroborated by the Si 2p data shown in figure 8.

Along with plasma annealing in vacuum, layers grown via all processes were also exposed to an atmospheric anneal and analysed using XPS so as to compare the two annealing methods. This annealing treatment results in Ti existing predominantly in the  $Ti^{4+}$  state with TD-T and TT-P exhibiting marginal contributions of  $Ti^{2+}$  and TT-T presenting  $Ti^{3+}$ . This is in line with what is to be expected, the plasma anneal being the

reducing environment causes the formation of oxygen vacancies resulting in the  $Ti^{3+}$  and  $Ti^{2+}$ . Annealing in atmosphere results in a  $Ti^{4+}$  dominant film as it moves towards a more stoichiometric state.

In order to further understand the impact of the surface treatments, we also analysed the Si 2p peaks for each sample. Figure 8 shows typical XPS spectra for the Si 2p core level of the titanium oxide films in their as-deposited state with atmospheric exposure, post plasma annealing also having been subsequently exposed to atmosphere and post air annealing stages. The presence of titanium silicates within the films shown in figure 8 is evident from the shift in BE position of the oxide peak which moves from higher to lower energy starting from approximately 103.8 eV in the case of bare  $SiO_2$ . With the air annealed sample showing the strongest contribution with XPS fitting of this peak showing the silicate contribution to be centred at a lower value of approximately 103 eV which is in line with literature values [34]. Figure 9 shows the change in BE separation of the Si 2p bulk and oxide peaks as a function of the number of ALD cycles and includes the post plasma and air annealed sample BE separations for all processes. This BE shift is also observed for sequential depositions as is seen from figure 3(b) where the shift of the  $Si^{4+}$  oxide peak to lower BE as a function of ALD cycles and can be attributed to the formation of interfacial Ti–Si–O bonds during the deposition of  $TiO_2$ , which have a lower BE than bulk  $SiO_2$  [35].

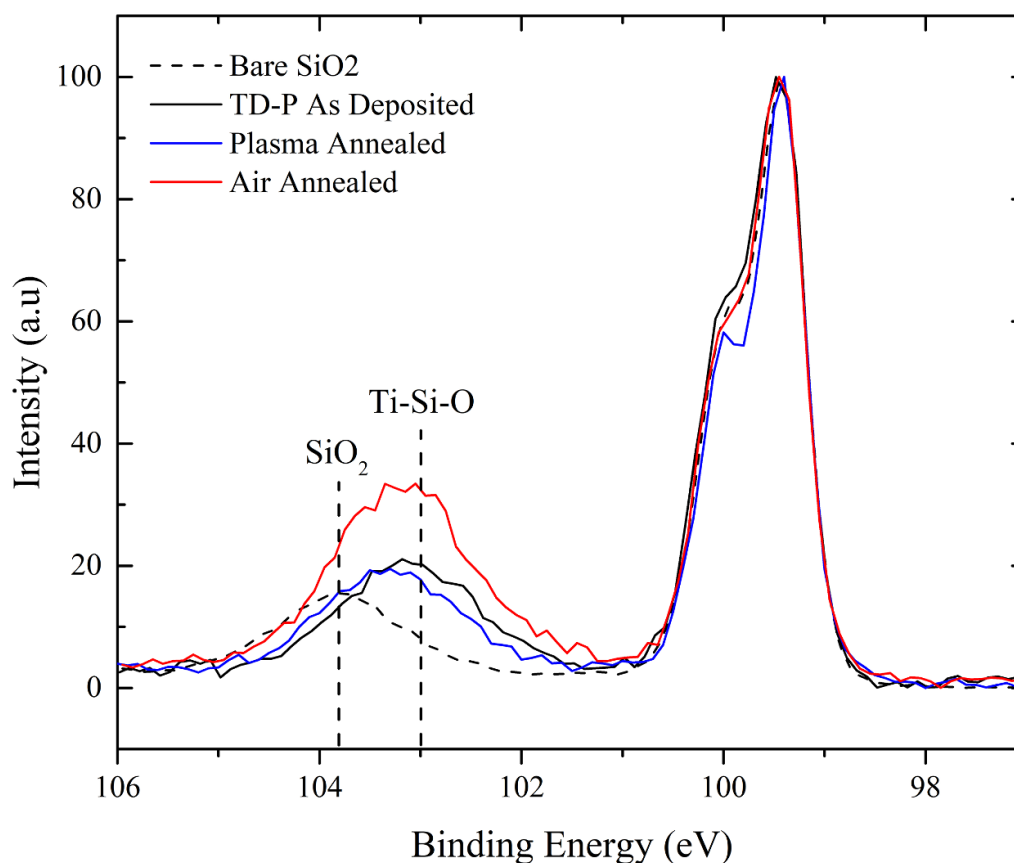


**Figure 8.** XPS high resolution spectra of the Si 2p region showing the evolution of the oxide peak with each stage of sample treatment with bare SiO<sub>2</sub> shown for reference.

In the case of TTIP grown by both PE-ALD and T-ALD, XPS core level spectra clearly show the presence of Ti 2p<sub>3/2</sub> and Ti 2p<sub>1/2</sub> peaks after the first half cycle. For TDMAT both processes show the presence of the Ti 2p<sub>1/2</sub> peak whereas the Ti 2p<sub>3/2</sub> signal-to-noise ratio is too low to clearly distinguish its precise position. However, it confirms that for both precursors and depositions processes that growth initiates as early as the first reactant dose. Additionally, during nucleation the Ti 2p peak exhibits high BE suggesting the dominance of the Ti<sup>4+</sup> state before shifting to lower BE with increasing ALD cycles during a sequential growth investigation. The shift is evident from figure 10 and it is seen to approach a limiting value in all process following 25 ALD cycles. A similar finding was reported by Methaapanon *et al* wherein the shift of the Ti 2p peak was shown for TiCl<sub>4</sub> samples grown via T-ALD with an approximate shift of the peak of 0.5 eV [35]. In the case of the TDMAT and TITP precursors investigated here we observe that for samples grown via PE-ALD the Ti 2p peak shifts by ~0.85 eV with T-ALD samples shifting by ~0.43 eV similar to that shown in the afore mentioned literature value. The behaviour of both the Si 2p and Ti 2p peaks during early-stage depositions can be explained by Si-O-Ti silicate bonds which form at the Si-Ti interface [35]. The BE positions of both peaks reduces from that of the stoichiometric 4+ oxide in both cases, in line with the reduced electronegativity of silicon and titanium when compared with oxygen. The behaviour

is consistent with that in figure 9 where the saturation of the BE separation is shown at ~25 cycles as well as with figure 10 where at 25 ALD cycles the shift in BE of the Ti 2p<sub>3/2</sub> also stabilises.

In the case of the O 1s spectra shown in figure 11, three discrete chemical states were identified. For all deposition processes in their as-deposited state (figure 11), the dominant peak corresponded to Ti-O bonding centred at approximately 531 eV. Plasma enhanced ALD processes yield a slightly lower BE, likely due to the formation of more titanium silicate and silicon suboxides than the thermal processes.

The peak observed in the O 1s spectra at 532.5 eV is attributed to remaining SiO<sub>x</sub> contribution, which is in line with prior reports [1, 10]. Note that the BE position of this peak also shifts from that of SiO<sub>2</sub> during sequential deposition in line with the above analysis (see supplemental information) Following H<sub>2</sub> plasma annealing (figure 11(b)) the oxygen peaks are observed to converge and align to 531 eV, whereas following air annealing a shift of all O 1s peaks to lower BE is observed. This is consistent with the Ti 2p spectra highlighted earlier, in that the reducing environment of the vacuum plasma anneal causes the creation of oxygen vacancies in the film which results in the Ti<sup>3+</sup> and Ti<sup>2+</sup> states. Whereas in the air annealing treatment (figure 11(c)) the abundance of oxygen in the atmosphere allows for the conversion of the film to Ti<sup>4+</sup>. In the as-deposited state not all processes showed their O 1s

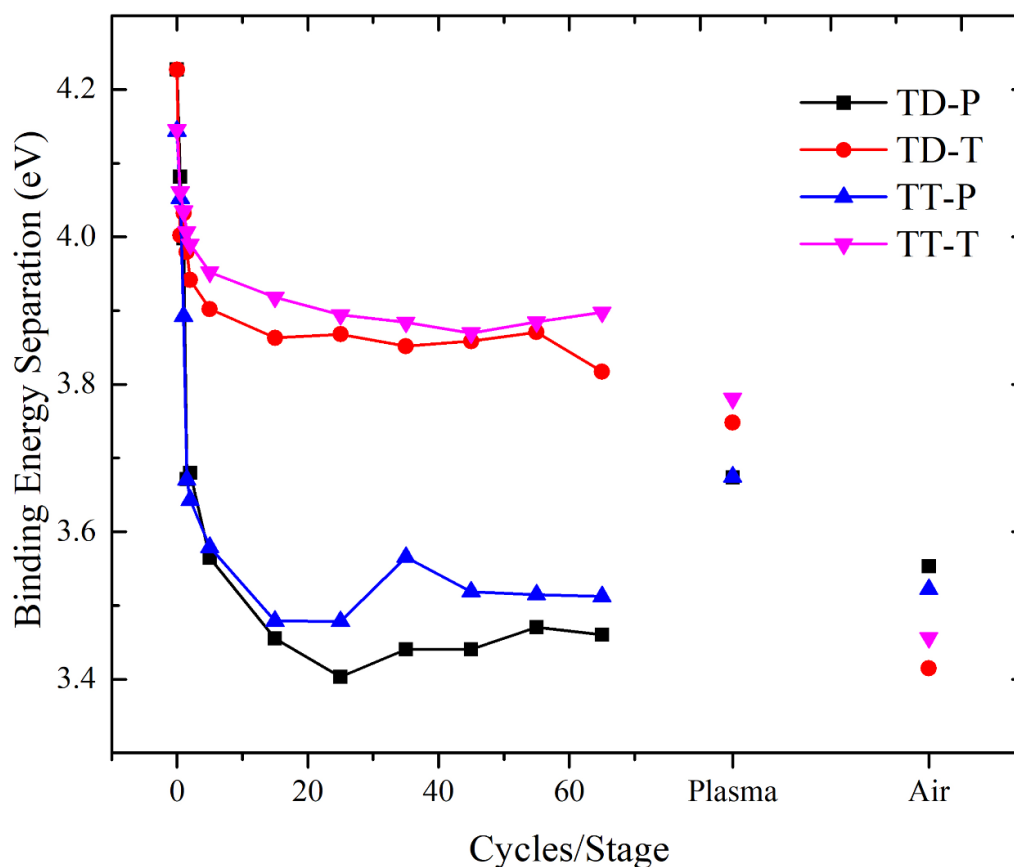


**Figure 9.** For all four growth processes the binding energy separation of the silicon oxide and bulk peak positions is shown as a function of increasing number of cycles for sequentially grown samples as well as positions for continuously grown 2 nm films following plasma and air annealing treatments. Data shown for plasma annealed samples followed exposure to atmosphere.

to be precisely aligned to O in TiO<sub>2</sub> and only after annealing in air did they conform suggesting incomplete reaction during the ALD deposition process.

### 3.4. Photoelectrochemical measurements

Following verification of film thickness using ellipsometry and XPS, 2 nm thick TiO<sub>2</sub> films were subjected to PEC testing to study the influence of ALD process parameters and post deposition annealing treatments on their electrical performance. A thickness of 2 nm has been widely identified as being an optimal thickness for photoanode performance enhancement [36]. Chronoamperometry tests were carried out using an applied voltage of 1 V vs Ag/AgCl which corresponds to 1.67 V vs the RHE, over a period of 100 s. Linear sweep voltammetry tests were carried out from 0 to 4.17 V vs RHE.

Figure 12 shows the current density for each sample at 1.23 V vs RHE for all four processes, extracted from a linear sweep voltammetry curve. It is clear from this figure that all growth processes benefitted greatly from post deposition annealing treatments, with the air annealing showing the most significant increase when compared to the as-deposited samples. Prior to annealing neither precursor, nor the choice of plasma enhanced or thermal ALD appeared to show consistent improvement performance over the others.

Examining the TiO<sub>2</sub> films in their as-deposited state shows a significant degradation in photocurrent over the short 100 s testing period, the extent of this degradation is shown in figure 13 wherein the amperometric performance of TDMAT PE-ALD films in their as-deposited, post plasma anneal and post annealing in atmosphere states are shown with the amperometric measurements for the remaining three processes shown in figure S6. This highlights the necessity for post deposition film treatments to stabilise currents and sustain high current output over an extended period of PEC operation. Most importantly from figure 13, a significant improvement in sample stability is seen in air annealed samples when compared to their plasma annealed counterparts. This a good demonstration of the superior performance, both in terms of gross photocurrent output, along with ability to sustain this increased output, of annealed over as-deposited counterparts.

This is followed by the plasma annealed sample which exhibits a high initial output current however, its output rapidly decreases after just 10 s of testing before beginning to stabilize at approximately 70  $\mu\text{A cm}^{-2}$ . The H<sub>2</sub> plasma annealed sample stability shows improved performance over as-deposited films when comparing start and end current output as an indication of stability. Although beginning at an initially high current competing even with that of the

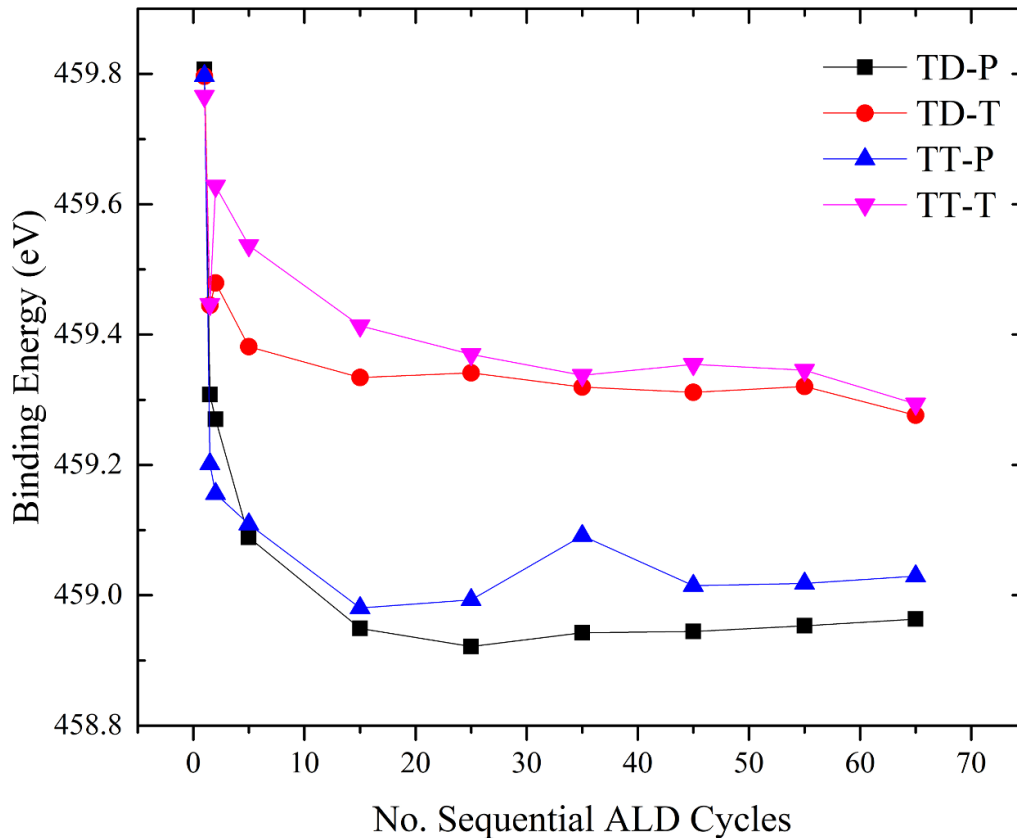


**Figure 10.** Shift of the Ti  $2p_{3/2}$   $Ti^{4+}$  peak binding energy position from 1 to 25 ALD cycles.

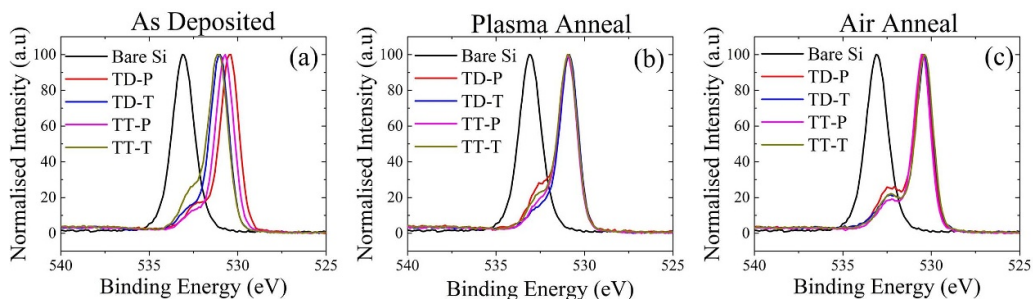


**Figure 11.** O 1s spectra of as-deposited, plasma annealed and air annealed samples showing the shift in oxygen binding energy as a function of their annealing environment.

plasma annealed sample, the as-deposited film showed a sharp decrease in current density in as little as 20 s.

These stability improvements are in line with findings from Hannula *et al* where they show vacuum annealing of titania films at 500 °C results in superior performance than is achieved by similar films which have received plasma annealing, no anneal or annealing at a reduced temperature of 400 °C [1]. All processes exhibit results which follow this pattern of air annealed samples outperforming the alternate treatments.

This PEC testing illustrates the performance enhancements obtained through applying post deposition treatments, with the air annealing of all samples producing the highest current output for all deposition processes.

#### 4. Discussion

Overall,  $H_2$  plasma annealing results in an almost  $3\times$  increase in photocurrent over as-deposited samples and a  $4\times$  increase in the case of air annealing. In the context of the XPS analysis in this work, we have shown significant differences in the spectra of all elements following annealing. In the context of plasma annealed films, the main observation is the presence of a 2+ and 3+ component in the Ti 2p spectra indicating the presence of oxygen vacancies in the films. Improved charge transport through insulating and semiconducting films is often linked to oxygen vacancies in the material. Density functional theory calculations using Quantum Espresso show that removing an

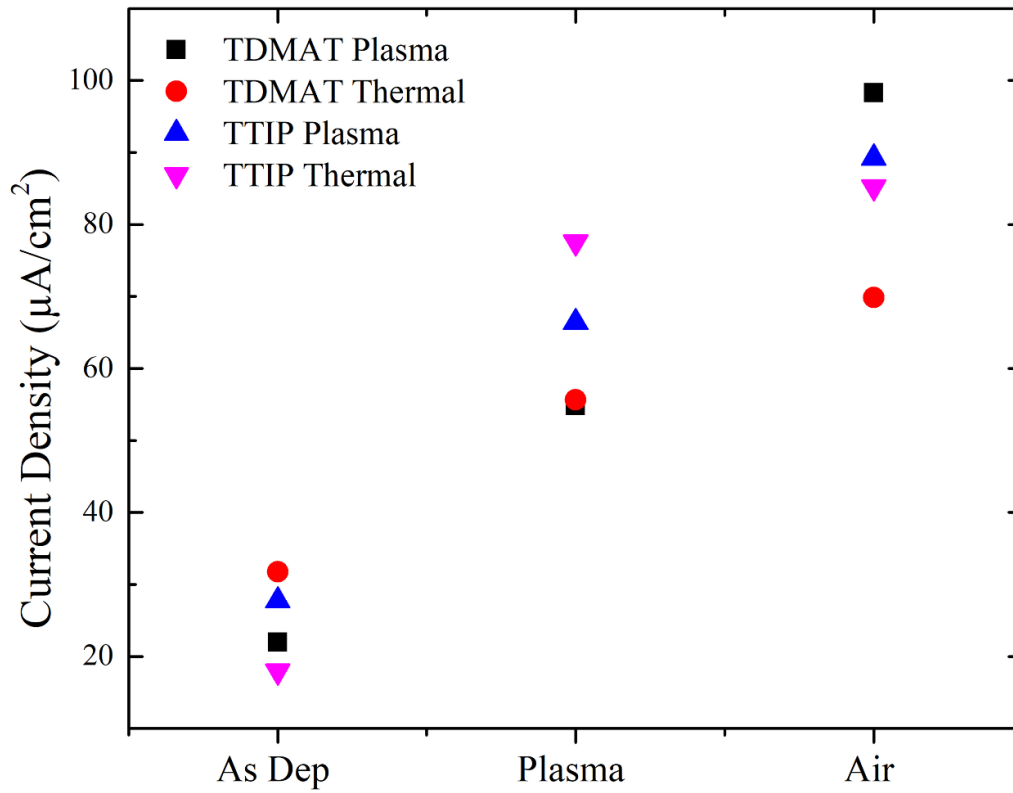


**Figure 12.** Cyclic voltammetry measured photocurrent at 1.23 V vs RHE as a function of sample treatment stage.

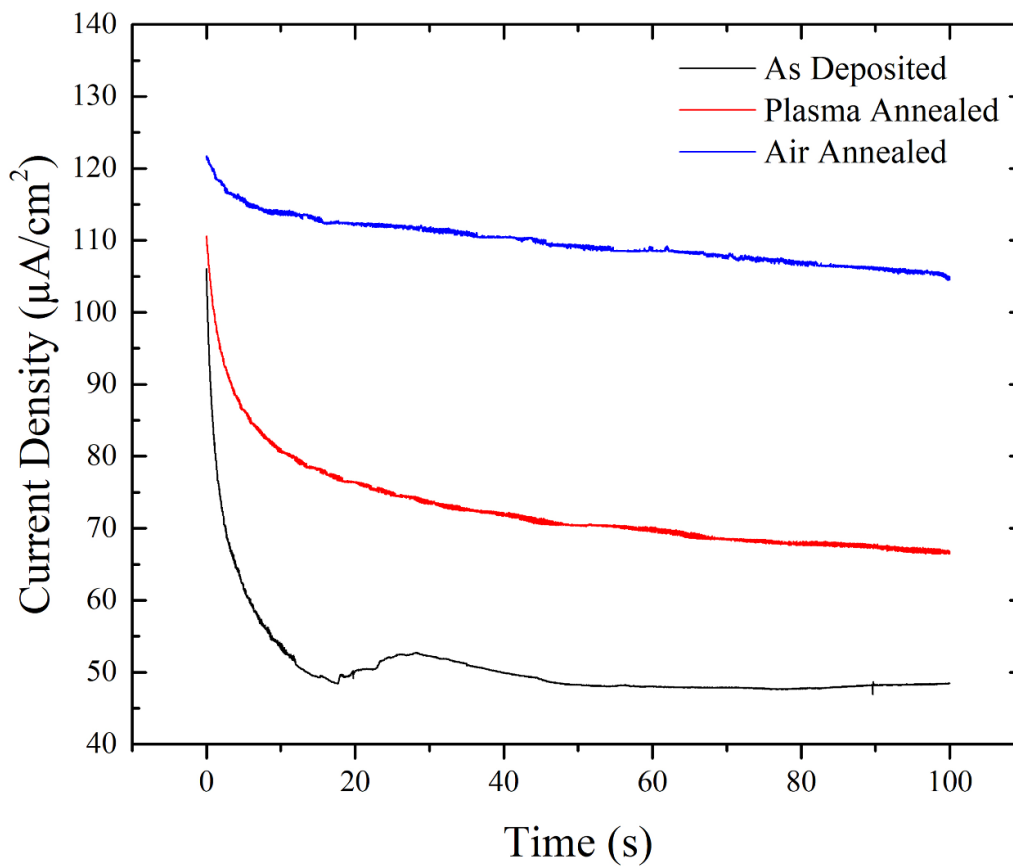


**Figure 13.** Exemplar amperometric curves from all treatment stages of TDMAT PEALD illustrating the air annealed sample has the greatest and most sustained output.

oxygen atom from the TiO<sub>2</sub> unit cell yields an increase in Ti d and O p states approximately 0.5 eV above the water oxidation energy (see figure S7) which would explain the increased photocurrent observed in figure 12 for the H<sub>2</sub> plasma annealed samples which causes a reduction of the TiO<sub>2</sub>. XPS valence band spectra (not shown) confirm an increased density of states approximately 2 eV above the Fermi energy.

However, this does not explain why air annealing should further increase the photocurrent, as we have observed that air annealing yields stoichiometric TiO<sub>2</sub> with no mid-gap states present.

The main difference in the film chemistry between the plasma and air annealed samples can be concluded from an analysis of figures 8 and 9. There is a significant increase in titanium silicate growth following atmospheric annealing, and the BE separation between the silicon bulk and oxide peaks reduce by approximately 0.2 eV. The BE position of the Si 2p oxide peak is similar to that of films grown by plasma enhanced ALD with no annealing treatment. From this we can conclude that we see more titanium silicate growth during PE-ALD than thermal ALD, but an atmospheric anneal results in significant silicate growth regardless of the deposition process. When comparing the area of the bulk and oxide peaks for the air annealed sample in figure 8, the relative areas are consistent with what one would observe for an SiO<sub>2</sub> film of approximately 2 nm, suggesting that there is almost complete conversion to titanium silicate.

The correlation between the growth of titanium silicate and improved photoelectrochemical performance and stability suggests that for ultra-thin films that a high temperature anneal to enable the conversion of the mixed phase material to titanium silicate is necessary in order to maximise photocurrent from silicon photoanodes protected by such thin films.

Furthermore, following such a treatment films grown using both precursors and by both ALD methods become chemically indistinguishable.

## 5. Conclusion

The presented results show an *in-situ* study on the deposition of amide and alkoxide precursors grown via PE-ALD and T-ALD processes, in contrast to some previous literature reports which detail only the comparison of two precursors for a single growth process or vice versa. Characterisation of these deposition processes with *in-situ* XPS allows for unique understandings of film chemistry in their as-deposited states without the added complexity of film contamination via atmospheric exposure while sequential growth of all processes allowed for precise monitoring of film nucleation. With PE-ALD grown TDMAT showing the most consistent growth, while T-ALD grown TTIP exhibited evidence of nucleation delay followed later by enhanced growth.

The application of post deposition annealing treatments were revealed through photoelectrochemical testing to enhance both current output and stability under test conditions. Of the annealing treatments, air annealing at 500 °C for 1 h yielded both the most stable and efficient titania films

grown from either precursor material and deposition process with plasma grown films showing only marginally higher current outputs versus thermally grown films.

## Data availability statement


The data that support the findings of this study are available upon reasonable request from the authors.

## Acknowledgments

The authors acknowledge funding from the Sustainable Energy Authority of Ireland Research Development and Demonstration Fund under Grant Number 18/RDD/185.

## ORCID iDs

S O'Donnell  <https://orcid.org/0000-0001-5194-0455>

M Snelgrove  <https://orcid.org/0000-0003-0344-1146>

R O'Connor  <https://orcid.org/0000-0001-5794-6188>

## References

- [1] Hannula M, Ali-Löytty H, Lahtonen K, Sarlin E, Saari J and Valden M 2018 Improved stability of atomic layer deposited amorphous TiO<sub>2</sub> photoelectrode coatings by thermally induced oxygen defects *Chem. Mater.* **30** 1199–208
- [2] van de Krol R and Grätzel M 2012 *Electronic Materials: Science & Technology* ed R van de Krol and M Grätzel (Berlin: Springer)
- [3] Walter M G, Warren E L, McKone J R, Boettcher S W, Mi Q, Santori E A and Lewis N S 2010 Solar water splitting cells *Chem. Rev.* **110** 6446–73
- [4] Hu S, Shaner M R, Beardslee J A, Lichterman M, Brunschwig B S and Lewis N S 2014 Amorphous TiO<sub>2</sub> coatings stabilize Si, GaAs, and GaP photoanodes for efficient water oxidation *Science* **344** 1005–9
- [5] Chen S and Wang L W 2012 Thermodynamic oxidation and reduction potentials of photocatalytic semiconductors in aqueous solution *Chem. Mater.* **24** 3659–66
- [6] Fujishima A and Honda K 1972 Electrochemical photolysis of water at a semiconductor electrode *Nature* **238** 37–38
- [7] Paracchino A, Laporte V, Sivula K, Grätzel M and Thimsen E 2011 Highly active oxide photocathode for photoelectrochemical water reduction *Nat. Mater.* **10** 456–61
- [8] Bard A J and Fox M A 1995 Artificial photosynthesis: solar splitting of water to hydrogen and oxygen *Acc. Chem. Res.* **28** 141–5
- [9] Lewis N S 2001 Light work with water *Nature* **414** 589–90
- [10] Bronneberg A C, Höhn C and Van De Krol R 2017 Probing the interfacial chemistry of ultrathin ALD-grown TiO<sub>2</sub> films: an in-line XPS study *J. Phys. Chem. C* **121** 5531–8
- [11] Scheuermann A G, Lawrence J P, Kemp K W, Ito T, Walsh A, Chidsey C E D, Hurley P K and McIntyre P C 2016 Design principles for maximizing photovoltage in metal-oxide-protected water-splitting photoanodes *Nat. Mater.* **15** 99–105
- [12] Zhuykov S, Akbari M K, Hai Z, Xue C, Xu H and Hyde L 2017 Wafer-scale fabrication of conformal atomic-layered TiO<sub>2</sub> by atomic layer deposition using tetrakis(dimethylamino) titanium and H<sub>2</sub>O precursors *Mater. Des.* **120** 99–108

- [13] Pore V, Heikkilä M, Ritala M, Leskelä M and Areva S 2006 Atomic layer deposition of TiO<sub>2</sub>-xNx thin films for photocatalytic applications *J. Photochem. Photobiol. A* **177** 68–75
- [14] Lakomaa E-L, Haukka S and Suntola T 1992 Atomic layer growth of TiO<sub>2</sub> on silica *Appl. Surf. Sci.* **60–61** 742–8
- [15] Jang M-H and Lei Y 2020 Ultrasonic atomization of titanium isopropoxide at room temperature for TiO<sub>2</sub> atomic layer deposition *J. Vac. Sci. Technol. A* **38** 062405
- [16] Sperling B A, Kimes W A and Maslar J E 2014 Quantitative infrared spectroscopy of tetrakis(dimethylamido)titanium for process measurements *ECS J. Solid State Sci. Technol.* **3** P26–31
- [17] Herrera-Gomez A, Bravo-Sanchez M, Ceballos-Sanchez O and Vazquez-Lepe M O 2014 Practical methods for background subtraction in photoemission spectra *Surf. Interface Anal.* **46** 897–905
- [18] Himpfel F J, McFeely F R, Taleb-Ibrahimi A, Yarmoff J A and Hollinger G 1988 Microscopic structure of the SiO<sub>2</sub>/Si interface *Phys. Rev. B* **38** 6084–96
- [19] Cumpson P J and Zalm P C 2000 Thickogram: a method for easy film thickness measurement in XPS *Surf. Interface Anal.* **29** 403–6
- [20] Wagner C D, Davis L E, Zeller M V, Taylor J A, Raymond R H and Gale L H 1981 Empirical atomic sensitivity factors for quantitative analysis by electron spectroscopy for chemical analysis *Surf. Interface Anal.* **3** 211–25
- [21] Powell C J and Jablonski A 2002 The NIST electron effective-attenuation-length database *J. Surf. Anal.* **9** 322–5
- [22] Adeloju S B 2005 Amperometry *Encyclopedia of Analytical Science* 2nd edn, ed P Worsfold, A Townshend and C Poole (Amsterdam: Elsevier) pp 70–79
- [23] Nečas D and Klapetek P 2012 Gwyddion: an open-source software for SPM data analysis *Cent. Eur. J. Phys.* **10** 181–8
- [24] Erdem B, Hunsicker R A, Simmons G W, David Sudol E, Dimonie V L and El-Aasser M S 2001 XPS and FTIR surface characterization of TiO<sub>2</sub> particles used in polymer encapsulation *Langmuir* **17** 2664–9
- [25] Smieszek A, Seweryn A, Marcinkowska K, Sikora M, Lawniczak-Jablonska K, Witkowski B S, Kuzmiuk P, Godlewski M and Marycz K 2020 Titanium dioxide thin films obtained by atomic layer deposition promotes osteoblasts' viability and differentiation potential while inhibiting osteoclast activity—potential application for osteoporotic bone regeneration *Materials* **13** 1–20
- [26] Harvey S P, Zhang F, Palmstrom A, Luther J M, Zhu K and Berry J J 2019 Mitigating measurement artifacts in TOF-SIMS analysis of perovskite solar cells *ACS Appl. Mater. Interfaces* **11** 30911–8
- [27] Jeynes C and Colaux J L 2016 Thin film depth profiling by ion beam analysis *Analyst* **141** 5944–85
- [28] Jackman M J, Thomas A G and Muryn C 2015 Photoelectron spectroscopy study of stoichiometric and reduced anatase TiO<sub>2</sub>(101) surfaces: the effect of subsurface defects on water adsorption at near-ambient pressures *J. Phys. Chem. C* **119** 13682–90
- [29] Marchant S and Foot P J S 1995 Poly(3-hexylthiophene)-zinc oxide rectifying junctions *J. Mater. Sci., Mater. Electron.* **6** 144–8
- [30] Dufond M E, Diouf M W, Badie C, Laffon C, Parent P, Ferry D, Grosso D, Kools J C S, Elliott S D and Santinacci L 2020 Quantifying the extent of ligand incorporation and the effect on properties of TiO<sub>2</sub> thin films grown by atomic layer deposition using an alkoxide or an alkylamide *Chem. Mater.* **32** 1393–407
- [31] Coster D and Kronig R D L 1935 New type of auger effect and its influence on the x-ray spectrum *Physica* **2** 13–24
- [32] Di Valentin C, Pacchioni G and Selloni A 2009 Reduced and n-type doped TiO<sub>2</sub>: nature of Ti<sup>3+</sup> species *J. Phys. Chem. C* **113** 20543–52
- [33] Khomenko V M, Langer K, Rager H and Fett A 1998 Electronic absorption by Ti<sup>3+</sup> ions and electron delocalization in synthetic blue rutile *Phys. Chem. Miner.* **25** 338–46
- [34] Brassard D, El Khakani M A and Ouellet L 2007 Substrate biasing effect on the electrical properties of magnetron-sputtered high-k titanium silicate thin films *J. Appl. Phys.* **102** 034106
- [35] Methaapanon R and Bent S F 2010 Comparative study of titanium dioxide atomic layer deposition on silicon dioxide and hydrogen-terminated silicon *J. Phys. Chem. C* **114** 10498–504
- [36] Bras J A 2015 Understanding Titanium Dioxide Passivation on Silicon Photoanodes in Photoelectrochemical Cells *MSc* Delft University of Technology